Cation Ordering in Layered O3 Li[Ni$_x$Li$_{1/3-2x/3}$Mn$_{2/3-x/3}$]O$_2$ (0 ≤ x ≤ $^1/_2$) Compounds

Y. S. Meng,[†,‡] G. Ceder,[†,‡] C. P. Grey,[§] W.-S. Yoon,[‖] M. Jiang,[§] J. Bréger,[§] and
Y. Shao-Horn*[,⊥]

*Advanced Materials for Micro- & Nano-Systems, Singapore−MIT Alliance, Singapore 117576,
Department of Materials Science and Engineering, Massachusetts Institute of Technology,
Cambridge, Massachusetts 02139, Department of Chemistry, SUNY Stony Brook,
Stony Brook, New York 11794, Materials Science Division, Brookhaven National Laboratory,
Upton, New York 11973, and Department of Mechanical Engineering,
Massachusetts Institute of Technology, Cambridge, Massachusetts 02139*

Received December 18, 2004. Revised Manuscript Received February 23, 2005

Three layered compounds, Li[Ni$_{1/2}$Mn$_{1/2}$]O$_2$ (x = $^1/_2$), Li[Li$_{1/9}$Ni$_{1/3}$Mn$_{5/9}$]O$_2$ (x = $^1/_3$), and Li$_2$MnO$_3$ (x = 0) of the Li[Ni$_x$Li$_{1/3-2x/3}$Mn$_{2/3-x/3}$]O$_2$ series were studied by electron diffraction in combination with synchrotron X-ray powder diffraction analyses. In-plane $\sqrt{3}\boldsymbol{a}_{\text{hex.}} \times \sqrt{3}\boldsymbol{a}_{\text{hex.}}$ ordering was found in all three samples, and a likely model for the occupancies of Li$^+$, Ni^{2+}, and Mn^{4+} on the sublattices of the transition metal layer was proposed. Perpendicular to the $\boldsymbol{c}_{\text{hex.}}$ axis, the ordered transition metal layers in the layered Li[Ni$_{1/2}$Mn$_{1/2}$]O$_2$ and Li[Li$_{1/9}$Ni$_{1/3}$Mn$_{5/9}$]O$_2$ crystals could be arranged mostly in the $P3_112$ stacking with some $C2/m$ stacking (such as *abab*...) abnormally. It is believed that the nickel ions in the lithium layer of these two samples play an important role in the stacking of transition metal layers. Moreover, electron diffraction analyses suggested that individual Li$_2$MnO$_3$ crystals that were obtained at 850 °C had at least two different $C2/m$ stacking sequence variants (*abab*..., *caca*..., and *cbcb*...) coexisting along the $\boldsymbol{c}_{\text{hex.}}$ axis, which were associated with the presence of some $P3_112$ stacking abnormally.

Introduction

Layered compounds of the Li[Ni$_x$Li$_{1/3-2x/3}$Mn$_{2/3-x/3}$]O$_2$ (0 ≤ x ≤ $^1/_2$) series, with alternating lithium layers and transition metal rich layers separated by close-packed oxygen arrays, have been studied extensively as potential positive electrode materials to replace LiCoO$_2$ for lithium rechargeable batteries in recent years.[1−14] The nickel content in the nominal compositions of these materials increases from x = 0 in Li$_2$MnO$_3$ {Li[Li$_{1/3}$Mn$_{2/3}$]O$_2$} to x = $^1/_2$ in Li[Ni$_{1/2}$Mn$_{1/2}$]O$_2$ upon substitution of lithium and manganese ions in the layered structure, as shown in Figure 1. These materials with x ≥ 1/3 not only have excellent reversible capacities but also improved thermal stability.[1,5,7] It have been shown that upon lithium removal Ni^{2+} is oxidized to Ni^{4+} and Mn^{4+} remains unchanged,[5,8,9,15] above an average oxidation state of 3.5 necessary for a stable MnO$_6$ coordination, which is associated with the structural stability of the layered structure of Li$_y$[Ni$_x$Li$_{1/3-2x/3}$Mn$_{2/3-x/3}$]O$_2$ during electrochemical cycling relative to the spinel form, unlike layered LiMnO$_2$.[16−18] The electrochemical behavior of these electrode materials is sensitive to nickel content, synthesis precursors, synthesis temperature, heat-treatment time, and cooling rates,[2,3,5,7] which could be attributed to different cation arrangements in the layered structure. In this paper, we discuss three aspects of cation arrangements of Li[Ni$_x$Li$_{1/3-2x/3}$Mn$_{2/3-x/3}$]O$_2$ compounds, as follows: (1) lithium and nickel interlayer mixing,

---

[*] To whom correspondence should be addressed. Fax: (617) 253-5981. E-mail: shaohorn@mit.edu.
[†] Singapore-MIT Alliance.
[‡] Department of Materials Science and Engineering, Massachusetts Institute of Technology.
[§] SUNY Stony Brook.
[‖] Brookhaven National Laboratory.
[⊥] Department of Mechanical Engineering, Massachusetts Institute of Technology.

(1) Ohzuku, T.; Makimura, Y. *Chem. Lett.* **2001**, *30*, 744−745.
(2) Makimura, Y.; Ohzuku, T. *J. Power Sources* **2003**, *119*, 156−160.
(3) Lu, Z. H.; Chen, Z. H.; Dahn, J. R. *Chem. Mater.* **2003**, *15*, 3214−3220.
(4) Johnson, C. S.; Kim, J. S.; Kropf, A. J.; Kahaian, A. J.; Vaughey, J. T.; Fransson, L. M. L.; Edstrom, K.; Thackeray, M. M. *Chem. Mater.* **2003**, *15*, 2313−2322.
(5) Lu, Z. H.; MacNeil, D. D.; Dahn, J. R. *Electrochem. Solid State Lett.* **2001**, *4*, A191−A194.
(6) Lu, Z. H.; Dahn, J. R. *J. Electrochem. Soc.* **2002**, *149*, A815−A822.
(7) Lu, Z. H.; Beaulieu, L. Y.; Donaberger, R. A.; Thomas, C. L.; Dahn, J. R. *J. Electrochem. Soc.* **2002**, *149*, A778−A791.
(8) Yoon, W. S.; Paik, Y.; Yang, X. Q.; Balasubramanian, M.; McBreen, J.; Grey, C. P. *Electrochem. Solid State Lett.* **2002**, *5*, A263−A266.
(9) Yoon, W. S.; Grey, C. P.; Balasubramanian, M.; Yang, X. Q.; McBreen, J. *Chem. Mater.* **2003**, *15*, 3161−3169.
(10) Grey, C. P.; Yoon, W. S.; Reed, J.; Ceder, G. *Electrochem. Solid State Lett.* **2004**, *7*, A290−A293.
(11) Meng, Y. S.; Ceder, G.; Grey, C. P.; Yoon, W. S.; Shao-Horn, Y. *Electrochem. Solid State Lett.* **2004**, *7*, A155−A158.
(12) Yoon, W. S.; Iannopollo, S.; Grey, C. P.; Carlier, D.; Gorman, J.; Reed, J.; Ceder, G. *Electrochem. Solid State Lett.* **2004**, *7*, A167−A171.
(13) Kim, J. S.; Johnson, C. S.; Vaughey, J. T.; Thackeray, M. M.; Hackney, S. A. *Chem. Mater.* **2004**, *16*, 1996−2006.
(14) Reed, J.; Ceder, G. *Electrochem. Solid State Lett.* **2002**, *5*, A145−148.
(15) Arachi, Y.; Kobayachi, H.; Emura, S.; Nakata, Y.; Tanaka, M.; Asai, T. *Chem. Lett.* **2003**, *32*, 60−61.
(16) Vitins, G.; West, K. *J. Electrochem. Soc.* **1997**, *144*, 2587−2592.
(17) Shao-Horn, Y.; Hackney, S. A.; Armstrong, A. R.; Bruce, P. G.; Gitzendanner, R.; Johnson, C. S.; Thackeray, M. M. *J. Electrochem. Soc.* **1999**, *146*, 2404−2412.
(18) Reed, J.; Ceder, G.; Van Der Ven, A. *Electrochem. Solid-State Lett.* **2001**, *4*, A78−A81.

10.1021/cm047779m CCC: $30.25
PAGE EST: 8.6

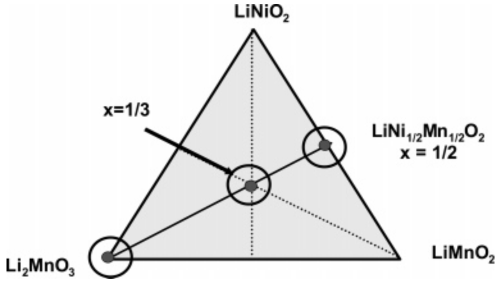

Figure 1. Ternary phase diagram of $LiNiO_2-LiMnO_2-Li_2MnO_3$. The solid line inside the triangle represents the solid solution $Li[Ni_xLi_{1/3-2x/3}Mn_{2/3-x/3}]O_2$ ($0 \le x \le {}^1/_2$).

where nickel moves to the lithium layer and the same amount of lithium moves to the transition metal layers; (2) in-plane ordering of lithium, manganese, and nickel in the transition metal rich layers; and (3) the stacking sequences of in-plane ordered layers.

Some fraction of nickel ions has shown to reside in the lithium layers[7,19] and the fraction is the highest in $Li[Ni_{1/2}Mn_{1/2}]O_2$ (around 9−12%) as the degree of nickel and lithium interlayer mixing (exchange) decreases as the nickel content x in $Li[Ni_xLi_{1/3-2x/3}Mn_{2/3-x/3}]O_2$ is reduced. In addition, the extent of the mixing has been reported to decrease as the synthesis temperature increases from 900 to 1000 °C.[3]

Given the charge difference between Li^+ and Mn^{4+}, one expects a strong ordering tendency between these ions. In-plane ordering of lithium and transition metal ions for compositions between $Li[Li_{1/9}Ni_{1/3}Mn_{5/9}]O_2$ ($x = {}^1/_3$) and Li_2MnO_3 {$Li[Li_{1/3}Mn_{2/3}]O_2$, $x = 0$} has been evidenced by X-ray diffraction,[3,20,21] solid-state nuclear magnetic resonance (NMR),[12] and extended X-ray absorption fine structure (EXAFS) studies.[22] In the $Li[Li_{1/3}Mn_{2/3}]O_2$ structure, the ordering of Li^+ and Mn^{4+} with a ratio (1:2) on the trigonal lattice leads to the formation of two distinct crystallographic α and β sites and thus a $\sqrt{3}\boldsymbol{a}_{hex.} \times \sqrt{3}\boldsymbol{a}_{hex.}$ supercell as reported in $Li_{0.33}CoO_2$[23,24] and $Li_{0.33}NiO_2$[25] associated with lithium and vacancy ordering, as shown in Figure 2a. It should be noted that the conventional cell definition of Li_2MnO_3[20] is monoclinic having space group $C2/m$, with $\boldsymbol{a}_{mon.} = 5.011$ Å ($\approx\sqrt{3}\boldsymbol{a}_{hex.}$), $\boldsymbol{b}_{mon.} = 8.679$ Å ($\approx 3\boldsymbol{a}_{hex.}$), and $\boldsymbol{c}_{mon.} = 5.105$ Å, $\beta_{mon.} = 109.46°$, as shown in Figure 2b. With the addition of nickel to the transition metal layer that now has a nominal composition of $Ni_xLi_{1/3-2x/3}Mn_{2/3-x/3}$, the $\sqrt{3}\boldsymbol{a}_{hex.} \times \sqrt{3}\boldsymbol{a}_{hex.}$ supercell having lithium and nickel on α, and nickel and manganese on β sites remains evident from X-ray powder diffraction analyses until x value reaches ${}^1/_3$.[3] NMR analysis of $Li[Ni_{1/2}Mn_{1/2}]O_2$ samples showed a much higher probability for Li^+ ions to be surrounded with 6 Mn^{4+} ions than would be found for a random solution. Using electron diffraction that is more sensitive to the difference in the scattering factor of α and β sites than X-rays, we have recently shown[11] that in-plane ordering in the $\sqrt{3}\boldsymbol{a}_{hex.} \times \sqrt{3}\boldsymbol{a}_{hex.}$ supercell exists in a $Li[Ni_{1/2}Mn_{1/2}]O_2$ sample, which consists of a considerable number of lithium ions in the transition metal layer as a result of the lithium and nickel interlayer exchange.

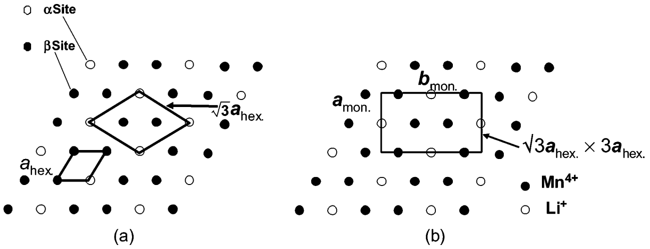

Figure 2. In-plane ordering of two different types of sites with a ratio of 1:2 (α sites in open circles and β sites in solid circles) on the trigonal lattice leads to the definition of (a) a $\sqrt{3}\boldsymbol{a}_{hex.} \times \sqrt{3}\boldsymbol{a}_{hex.}$ supercell (marked by lines) as reported in $Li_{0.33}CoO_2$[23,24] and $Li_{0.33}NiO_2$[25] or (b) an $\boldsymbol{a}_{mon.}$ ($\sim\sqrt{3}\boldsymbol{a}_{hex.}$) × $\boldsymbol{b}_{mon.}$ ($\sim 3\boldsymbol{a}_{hex.}$) supercell (marked by lines) as observed in Li_2MnO_3.

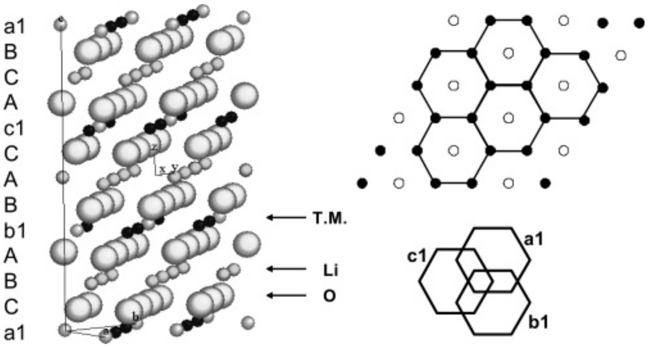

Figure 3. Transition metal layers of $Li[Ni_{1/2}Mn_{1/2}]O_2$ reported to have a stacking sequence of *a*1*b*1*c*1 *a*2*b*2*c*2 (or *ab abc*...) along the $\boldsymbol{c}_{hex.}$ axis with space group $P3_112$.[11]

Although the in-plane $\sqrt{3}\boldsymbol{a}_{hex.} \times \sqrt{3}\boldsymbol{a}_{hex.}$ ordering in $Li[Ni_{1/2}Mn_{1/2}]O_2$ is the same as that of Li_2MnO_3,[20,21] our previous studies[11] have shown that the stacking sequences of in-plane ordering perpendicular to the layers (along the $\boldsymbol{c}_{hex.}$ axis) of these two materials are different. $Li[Ni_{1/2}Mn_{1/2}]O_2$ adopts a stacking sequence of *a*1*b*1*c*1*a*2*b*2*c*2... (or *abcabc*...) along the $\boldsymbol{c}_{hex.}$ axis and the ordering reduces the symmetry from space group $R\bar{3}m$ for the parent hexagonal structure to $P3_112$, as shown in Figure 3. In contrast, the stacking sequence of in-plane ordering in Li_2MnO_3 {$Li[Li_{1/3}Mn_{2/3}]O_2$} with space group $C2/m$ reported previously[20,21] is *a*1*c*1*a*2*c*2... (*acac*...), *a*1*b*1*a*2*b*2... (*abab*...), or *b*1*c*1*b*2*c*2... (*bcbc*...) along the $\boldsymbol{c}_{hex.}$ axis, as shown in Figure 4. The crystallographic relationship between the parent hexagonal cell with space group $R\bar{3}m$ and the monoclinic cell of Li_2MnO_3 with space group $C2/m$ is shown in Figure 5. As the shift of origin in direct space does not affect the transformation of Miller indices of atomic planes nor the indices of directions in direct space, a common origin (a shift of conventional Li_2MnO_3 cell origin) is chosen in order to simply show the relative orientation relationship of these two cells.

To understand how the in-plane cation ordering and stacking sequences of in-plane ordering change as a function

---

(19) Kobayashi, H.; Sakaebe, H.; Kageyama, H.; Tatsumi, K.; Arachi, Y.; Kamiyama, T. *J. Mater. Chem.* **2003**, *13*, 590−595.

(20) Strobel, P.; Lambertandron, B. *J. Solid State Chem.* **1988**, *75*, 90−98.

(21) Massarotti, V.; Bini, M.; Capsoni, D.; Altomare, A.; Moliterni, A. G. G. *J. Appl. Crystallogr.* **1997**, *30*, 123−127.

(22) Yoon, W.-S.; Kim, N.; Yang, X.-Q.; McBreen, J.; Grey, C. P. *J. Power Sources* **2003**, *119*−*121*, 649−653.

(23) Van der Ven, A.; Aydinol, M. K.; Ceder, G.; Kresse, G.; Hafner, J. *Phys. Rev. B* **1998**, *58*, 2975−2987.

(24) Shao-Horn, Y.; Levasseur, S.; Weill, F.; Delmas, C. *J. Electrochem. Soc.* **2003**, *150*, A366−A373.

(25) Delmas, C.; Menetrier, M.; Croguennec, L.; Levasseur, S.; Peres, J. P.; Pouillerie, C.; Prado, G.; Fournes, L.; Weill, F. *Int. J. Inorg. Mater.* **1999**, *1*, 11−19.

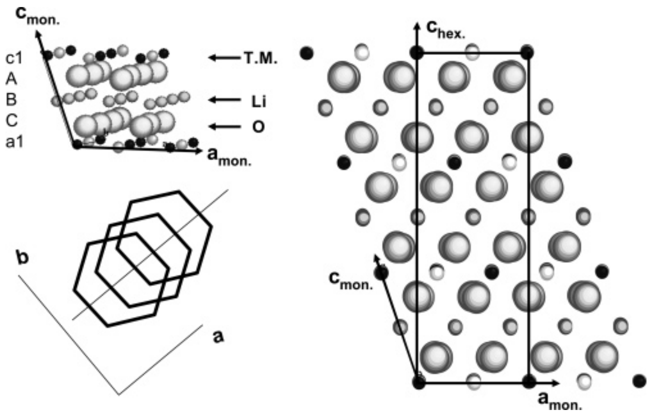

Figure 4. Transition metal layers of Li_2MnO_3 reported to have a stacking sequence of *a*1*c*1*a*2*c*2 (*acac*...), or *a*1*b*1*a*2*b*2 (*abab*...), or *b*1*c*1*b*2*c*2 (*bcbc*...) perpendicular to the $\boldsymbol{c}_{hex.}$ axis, with space group *C*2/*m*.[20,21]

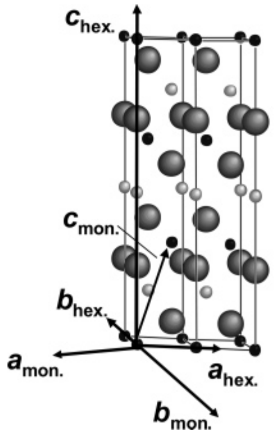

$$\begin{pmatrix} \vec{a}^*_{mon.} \\ \vec{b}^*_{mon.} \\ \vec{c}^*_{mon.} \end{pmatrix} = \begin{pmatrix} -0.5 & 0 & 1 \\ 0.167 & -0.333 & 0 \\ 0 & 0 & 3 \end{pmatrix} \begin{pmatrix} \vec{a}^*_{hex.} \\ \vec{b}^*_{hex.} \\ \vec{c}^*_{hex.} \end{pmatrix}$$

$$\begin{pmatrix} \vec{a}^*_{hex.} \\ \vec{b}^*_{hex.} \\ \vec{c}^*_{hex.} \end{pmatrix} = \begin{pmatrix} -2 & 0 & 2/3 \\ -1 & -3 & 1/3 \\ 0 & 0 & 1/3 \end{pmatrix} \begin{pmatrix} \vec{a}^*_{mon.} \\ \vec{b}^*_{mon.} \\ \vec{c}^*_{mon.} \end{pmatrix}$$

Figure 5. Crystallographic relationship between the parent hexagonal cell with space group $R\bar{3}m$ and the monoclinic cell of Li_2MnO_3 with space group *C*2/*m*. Note that a common origin is chosen as the shift of origin direct space does not affect the transformation of Miller indices of atomic planes or the indices of directions in direct space.

of lithium and nickel content in the transition metal layer of the Li[Ni$_x$Li$_{1/3-2x/3}$Mn$_{2/3-x/3}$]O_2 series, we use electron diffraction in this study to investigate three compounds with different nominal nickel fractions in the transition metal layer, $x = {}^1/_2$, $^1/_3$, and 0.

Experimental Section

Samples of Li[Ni$_{1/2}$Mn$_{1/2}$]O_2 ($x = 0$) and a Li[Ni$_{1/3}$Li$_{1/9}$Mn$_{5/9}$]O_2 ($x = {}^1/_3$) were synthesized from stoichiometric quantities of coprecipitated manganese and nickel hydroxides with lithium hydroxide at 900 °C for 24 h in O_2, and both were quenched to room temperature in liquid nitrogen. A Li_2MnO_3 sample was heat-treated at 850 °C for 24 h and cooled to room temperature in air.

The synchrotron X-ray powder diffraction patterns of Li[Ni$_{1/2}$Mn$_{1/2}$]O_2 and Li_2MnO_3 samples were collected on the beamline 32-ID at the Advanced Photo Source (Argonne National Laboratory, Chicago, IL). The powder samples placed in glass capillaries were characterized by X-rays with a wavelength of 0.4958 Å, and synchrotron diffraction data were collected from 4 to 50.9° with a fixed step of 0.001° (2θ) at room temperature. The synchrotron X-ray powder diffraction data of the Li[Ni$_{1/3}$Li$_{1/9}$Mn$_{1/2}$]O_2 sample was collected between 5 and 48.9° at a fixed step of 0.036° (2θ) with a wavelength of 0.9220 Å on the beamline X7B at the National Synchrotron Light Source (Brookhaven National Laboratory, Upton, NY). Rietveld refinements and profile matching of the powder diffraction data were performed using the program Fullprof[26] and the Winplotr interface. In our refinements, the oxygen occupancy is not refined and the default value is set as 2 for the layered structure with space group $R\bar{3}m$ in the Fullprof program. The Ni and Li occupancy were refined with the following constraints: (1) the Mn occupancy in the 3*a* sites is fixed to the stoichiometry, (2) the sum of Ni, Mn, and Li occupancy on the 3*a* sites is equal to 1, (3) the sum of Ni and Li occupancy on the 3*b* sites is equal to 1, and (4) 3*a* sites have one thermal parameter and 3*b* sites have one thermal parameter.

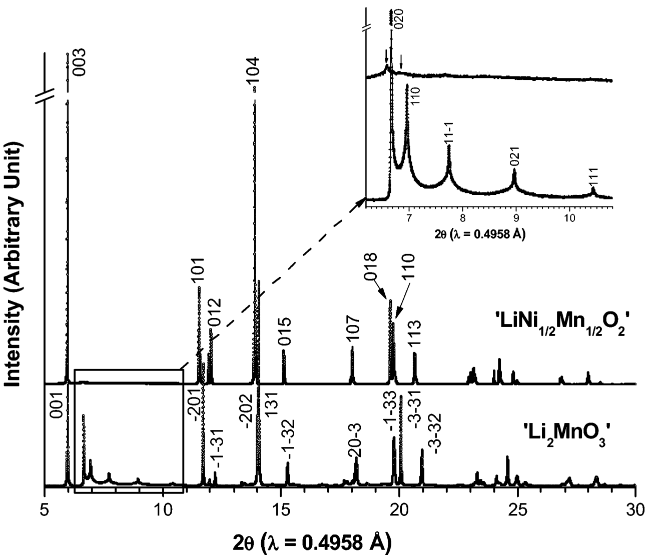

Figure 6. Synchrotron X-ray powder diffraction spectra of Li[Ni$_{1/2}$Mn$_{1/2}$]O_2 and Li_2MnO_3 samples.

Electron diffraction patterns and transmission electron microscope (TEM) images were collected from all three powder samples, which were suspended on a copper grid with lacey carbon under an accelerating voltage of 200 keV on a JEOL 200CX, JEOL 2000FX, or JEOL 2010 microscope. Chemical analyses of nickel and manganese contents of individual Li[Ni$_{1/2}$Mn$_{1/2}$]O_2 crystals were performed by X-ray energy dispersive spectroscopy (EDS) at a sample tilt angle of +15° (tilted toward the X-ray detector) on the JEOL 2010 microscope. Examination of 10 randomly selected single crystals revealed an average composition of $LiMn_{0.51}Ni_{0.49}O_2$, which agrees with the nominal composition within experimental uncertainty. Lithium and oxygen contents were not quantified by EDS and were assumed stoichiometric.

Results and Discussion

Synchrotron X-ray Powder Diffraction Analysis. Synchrotron X-ray diffraction data of the Li[Ni$_{1/2}$Mn$_{1/2}$]O_2 and Li_2MnO_3 powder samples, two end members of Li[Ni$_x$Li$_{1/3-2x/3}$Mn$_{2/3-x/3}$]O_2 composition series ($x = {}^1/_2$ and $x = 0$), are shown in Figure 6. Both samples were found phase pure. Major diffraction peaks of the Li[Ni$_{1/2}$Mn$_{1/2}$]O_2 sample are indexed according to the parent hexagonal structure with space group $R\bar{3}m$ and those of Li_2MnO_3 are indexed according to the conventional monoclinic cell[20,21] with space group *C*2/*m*.

Rietveld refinement results of the Li[Ni$_{1/2}$Mn$_{1/2}$]O_2 data are shown in Table 1. The lattice parameters of the parent layered structure with space group $R\bar{3}m$ were found, $\boldsymbol{a}_{hex.}$= 2.8873(1) Å and $\boldsymbol{c}_{hex.}$=14.2901(8) Å, which were consistent

---

(26) Rodriguez-Carvajal, J. In *Satellite Meeting on Powder Diffraction of the XV Congress of the IUCr* 127; International Union of Crystallography: Toulouse, France, 1990.

Table 1. Synchrotron X-ray Diffraction Data Acquisition Conditions and Rietveld Refinement Results of the $Li[Ni_{1/2}Mn_{1/2}]O_2$ Powder Sample[a]

	$LiNi_{1/2}Mn_{1/2}O_2$
space group	$R\bar{3}m$
$\boldsymbol{a}_{hex.}$ (Å)	2.8873(1)
$\boldsymbol{c}_{hex.}$ (Å)	14.2901(8)

atom	site	Wyckoff positions			occupancy	B (Å)
Ni(1)	3a	0	0	0	0.391	0.14(4)
Ni(2)	3b	0	0	0.5	0.109	0.8(3)
Mn	3a	0	0	0	0.5	0.14(4)
Li(1)	3b	0	0	0.5	0.891	0.8(3)
Li(2)	3a	0	0	0	0.109	0.14(4)
O	6c	0	0	0.257(6)	2	0.6(1)

angular range	$4° \leq 2\theta \leq 50.9°$
step size (deg)	0.001
X-ray radiation wavelength (Å)	0.4958
number of fitted parameters	16
pseudo-Voigt function	$PV = \eta_o L + (1 - \eta_o)G$ [b]
preferential orientation of the particles (the basal plane)	0.99(1)
reliability factors	$R_{wp} = 15.6\%$; $R_B = 5.77\%$

[a] The number in the parentheses of the refinement results such as 0.14(4) indicates that the third decimal place is uncertain and the standard deviation is equal to 0.004 in the case of 0.14(4). Standard deviation have been multiplied by the Scorr number to correct the local correlations.[26] [b] With $\eta_o = 0.51(7)$; $U = 0.034(8)$; $V = 0.006(2)$; $W = -0.0002(1)$.

Table 2. Synchrotron X-ray Diffraction Data Acquisition Conditions and Profile Matching Results of the Li_2MnO_3 Powder Sample[a]

	Li_2MnO_3
space group	$C2/m$
$\boldsymbol{a}_{mon.}$ (Å)	4.9261(5)
$\boldsymbol{b}_{mon.}$ (Å)	8.527(1)
$\boldsymbol{c}_{mon.}$ (Å)	5.0280(7)
β (deg)	109.22(1)
angular range	$4° \leq 2\theta \leq 50.9°$
step size (deg)	0.001
X-ray radiation wavelength (Å)	0.4958
number of fitted parameters	11
reliability factors	R_{wp}= 30.2%; $R_B = 3.90\%$

[a] Rietveld refinements were attempted but not successful.

with previous studies of materials prepared under similar synthesis conditions [$\boldsymbol{a}_{hex.}$= 2.889(4) Å and $\boldsymbol{c}_{hex.}$=14.29(3) Å].[7] In addition, our refinement showed that 10.9% of nickel was present in the lithium layer, which is in good agreement with previous neutron diffraction analyses of interlayer mixing of lithium and nickel ions (11−12%).[7] Therefore, the composition in the transition metal layer for the $Li[Ni_{1/2}Mn_{1/2}]O_2$ sample can be written as $[Li_{0.11}Ni_{0.39}Mn_{0.50}]$. As shown at the top right corner of Figure 6, the superlattice reflections associated with the $\sqrt{3}\boldsymbol{a}_{hex.} \times \sqrt{3}\boldsymbol{a}_{hex.}$ cation ordering are weak but visible in the $Li[Ni_{1/2}Mn_{1/2}]O_2$ powder spectrum. The presence of these superlattice reflections confirms the ordering of Li^+, Ni^{2+}, and Mn^{4+} in the transition metal layer as revealed previously by electron diffraction analyses.[11]

Profile matching of the synchrotron Li_2MnO_3 data showed that the structural parameters of the conventional monoclinic cell with space group $C2/m$ were $\boldsymbol{a}_{mon.}$= 4.926 Å, $\boldsymbol{b}_{mon.}$ = 8.527 Å, $\boldsymbol{c}_{mon.}$ = 5.028 Å, and β = 109.22°, as shown in Table 2. It should be noted that these parameters obtained in this study are slightly different from the values of previous single-crystal X-ray diffraction analyses ($\boldsymbol{a}_{mon.}$= 4.937 Å, $\boldsymbol{b}_{mon.}$ = 8.532 Å, $\boldsymbol{c}_{mon.}$ = 5.030 Å, and β = 109.46°).[20] In-plane ordering of Li^+ and Mn^{4+} (1:2) leads to deviation in the a/b ratio of the rhombohedral layered structure as the electrostatic interactions of Li^+ and Mn^{4+} ions differ along the $\boldsymbol{a}$ and $\boldsymbol{b}$ directions. The deviation in this ratio from the ideal value (1.732) decreases the crystal symmetry from rhombohedral to monoclinic, where the crystal structure can be modified by varying the a/b ratio and/or β. It is important to point out that the $a_{mon.}/b_{mon.}$ and β values of the Li_2MnO_3 sample in this study are 1.731 and 109.22°, which are closer to the ideal value (1.732 and 109.14° for the rhombohedral symmetry) than those of Li_2MnO_3 reported in the literature (single-crystal Li_2MnO_3, 1.728 and 109.46°;[20] and Li_2MnO_3 powder, 1.730 and 109.39° [21]). It is speculated that the difference in structural parameters could be attributed to the fact that the Li_2MnO_3 powder sample used in this study had slightly higher strains than the single-crystal and powder samples reported previously,[20,21] as evidenced by the broadening of selective superlattice peaks (Figure 6).

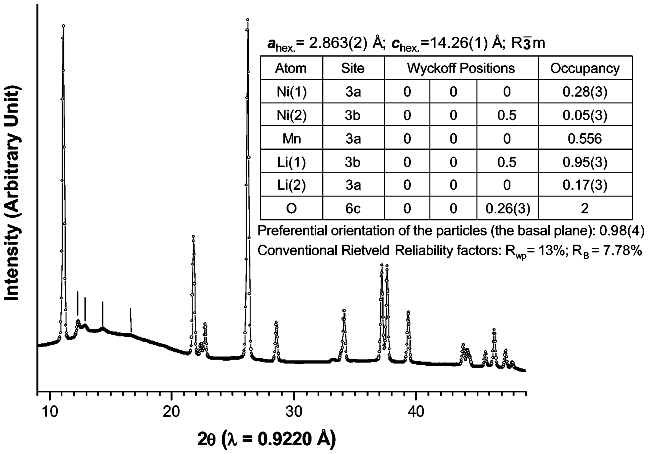

$\boldsymbol{a}_{hex.}$= 2.863(2) Å; $\boldsymbol{c}_{hex.}$=14.26(1) Å; $R\bar{3}m$

Atom	Site	Wyckoff Positions			Occupancy
Ni(1)	3a	0	0	0	0.28(3)
Ni(2)	3b	0	0	0.5	0.05(3)
Mn	3a	0	0	0	0.556
Li(1)	3b	0	0	0.5	0.95(3)
Li(2)	3a	0	0	0	0.17(3)
O	6c	0	0	0.26(3)	2

Preferential orientation of the particles (the basal plane): 0.98(4)

Conventional Rietveld Reliability factors: R_{wp}= 13%; R_B = 7.78%

Figure 7. Synchrotron X-ray powder diffraction spectra of the $Li[Ni_{1/3}Li_{1/9}Mn_{5/9}]O_2$ sample and the Rietveld refinement results. Four strong superstructure peaks are marked by arrows.

Rietveld refinements of the synchrotron data of the Li_2MnO_3 sample were attempted but the superstructure peaks associated with the ordering of Li^+ and Mn^{4+} in the $Li_{1/3}Mn_{2/3}$ layer in the range of $6° \leq 2\theta \leq 11°$ with selective, pronounced peak broadening and asymmetry could not be modeled successfully, as shown in the insert of Figure 6. Therefore, atomic positions and occupancies could not be refined with reasonable reliability factors. NMR analysis of this Li_2MnO_3 sample revealed that there was no or little evidence of in-plane Li^+ and Mn^{4+} mixing in the $Li_{1/3}Mn_{2/3}$ layer. It is proposed here that the selective broadening of these superlattice peaks is attributed to disorder in the stacking sequence of in-plane ordered $Li_{1/3}Mn_{2/3}$ layers (deviation from the normal stacking sequence, *acac*..., perpendicular to the layers) in the Li_2MnO_3 powder sample, which will be further explained in later sections.

Synchrotron X-ray diffraction data of the $Li[Ni_{1/3}Li_{1/9}Mn_{5/9}]O_2$ sample are shown in Figure 7. The lattice parameters of the parent layered structure with space group $R\bar{3}m$ were found, $\boldsymbol{a}_{hex.}$= 2.863 Å and $\boldsymbol{c}_{hex.}$= 14.26 Å, which is consistent with previous studies of materials prepared under similar synthesis conditions ($\boldsymbol{a}_{hex.}$= 2.875 Å and $\boldsymbol{c}_{hex.}$=14.279 Å].[7] In addition, our refinement showed that 5% of nickel was present in the lithium layer, which is in good agreement with

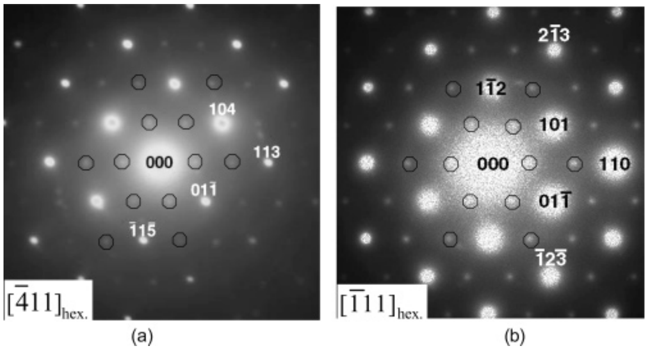

Figure 8. (a) [$\bar{4}$11]$_{hex.}$ and (b) [$\bar{1}$11]$_{hex.}$ electron diffraction patterns of Li[$Ni_{1/2}Mn_{1/2}$]O_2, which show the superstructure reflections consistent with the $\sqrt{3}\boldsymbol{a}_{hex.} \times \sqrt{3}\boldsymbol{a}_{hex.} \times \boldsymbol{c}_{hex.}$ superstructure with space group $P3_112$.

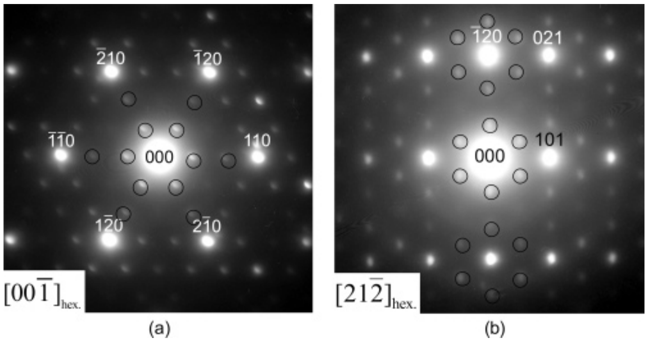

Figure 9. (a) [00$\bar{1}$]$_{hex.}$ and (b) the [21$\bar{2}$]$_{hex.}$ electron diffraction patterns of the Li[$Ni_{1/3}Li_{1/9}Mn_{5/9}$]O_2 sample, which show the superstructure reflections consistent with $\sqrt{3}\boldsymbol{a}_{hex.} \times \sqrt{3}\boldsymbol{a}_{hex.} \times \boldsymbol{c}_{hex.}$ superstructure with space group $P3_112$.

previous neutron diffraction analyses of interlayer mixing of lithium and nickel ions (6−7%).[7] Having more lithium in the transition metal layer and smaller values of x, the interlay mixing (exchange) of Ni^{2+} and Li^+ is reduced. Therefore, the composition in the transition metal layer of Li[$Ni_{1/3}Li_{1/9}Mn_{5/9}$]O_2 can be written as [$Li_{0.17}Ni_{0.28}Mn_{0.55}$]. Increased lithium fraction in the transition metal layer is consistent with the following observations that (1) superlattice reflections (marked by arrows in Figure 7) associated with the $\sqrt{3}\boldsymbol{a}_{hex.} \times \sqrt{3}\boldsymbol{a}_{hex.}$ cation ordering are stronger than those observed in the Li[$Ni_{1/2}Mn_{1/2}$]O_2 sample (Figure 6 inset) and (2) superlattice reflections were observed in all crystals studied while they were found only in 50% of the crystals analyzed from the Li[$Ni_{1/2}Mn_{1/2}$]O_2 sample.

Electron Diffraction Analysis. Electron diffraction studies of Li[$Ni_{1/2}Mn_{1/2}$]O_2 ($x = 1/2$), Li[$Ni_{1/3}Li_{1/9}Mn_{5/9}$]O_2 ($x = 1/3$), and Li_2MnO_3 ($x = 0$) revealed the same type of long-range ordering in the transition metal layer in all three samples.

Two representative electron diffraction patterns obtained from each of the Li[$Ni_{1/2}Mn_{1/2}$]O_2, Li[$Ni_{1/3}Li_{1/9}Mn_{5/9}$]O_2, and Li_2MnO_3 samples are shown in Figures 8−10, respectively. The fundamental reflections and the zone axes are indexed to the parent hexagonal cell with rhombohedral symmetry and space group $R\bar{3}m$. The most predominant feature of the electron diffraction patterns obtained from all three samples is that only the $(11\boldsymbol{l})_{hex.}$ planar spacings ($\boldsymbol{l} = 3n$, $n = 0, \pm1, \pm2...$) in the parent hexagonal structure are tripled by the presence of superlattice reflections. First-order and some second-order superlattice reflections are marked by circles in Figures 8−10.

Figure 8a and b show the [$\bar{4}$11]$_{hex.}$ and [$\bar{1}$11]$_{hex.}$ zone axis patterns collected from the Li[$Ni_{1/2}Mn_{1/2}$]O_2 sample, respectively. Consistent with what we reported previously,[11] the presence of these unique superstructure reflections indicated the presence of a $\sqrt{3}\boldsymbol{a}_{hex.} \times \sqrt{3}\boldsymbol{a}_{hex.} \times \boldsymbol{c}_{hex.}$ superstructure with space group $P3_112$. Such long-range ordering in the transition metal layer was observed in 50% of the crystals analyzed (17 single crystals out of total 34 crystals showed superlattice reflections and the others had only fundamental reflections).

Figure 9a and b show the [00$\bar{1}$]$_{hex.}$ and [21$\bar{2}$]$_{hex.}$ patterns, respectively, collected from one crystal in the Li[$Ni_{1/3}Li_{1/9}Mn_{5/9}$]O_2 ($x = 1/3$) sample. The superlattice reflections present can be indexed to the $\sqrt{3}\boldsymbol{a}_{hex.} \times \sqrt{3}\boldsymbol{a}_{hex.} \times \boldsymbol{c}_{hex.}$ superstructure. A total of 15 crystals of the Li[$Ni_{1/3}Li_{1/9}Mn_{5/9}$]O_2 sample were studied by electron diffraction, and superlattice reflections unique to the superstructure were found in all the crystals. Long-order ordering is more predominant in Li[$Ni_{1/3}Li_{1/9}Mn_{5/9}$]O_2 ($x = 1/3$) than Li[$Ni_{1/2}Mn_{1/2}$]O_2.

None of the electron diffraction patterns collected from 16 crystals in the Li_2MnO_3 sample could be indexed uniquely to the conventional monoclinic structure (shown in Figure 4) with space group $C2/m$. As the monoclinic distortion (the deviation of the $a_{mon.}/b_{mon.}$ ratio and β from their ideal values) in the Li_2MnO_3 sample is minute (as shown in Table 2), the difference in the interplanar spacing of atomic planes caused by this distortion is small, which is within experiment uncertainty of electron diffraction measurements. Therefore, to a first-order approximation, these experimental diffraction patterns can be indexed by the $\sqrt{3}\boldsymbol{a}_{hex.} \times \sqrt{3}\boldsymbol{a}_{hex.} \times \boldsymbol{c}_{hex.}$ superstructure with space group $P3_112$ by neglecting the monoclinic distortion, from which the type of cation ordering in the layered structure can be examined and compared with that in Li[$Ni_{1/2}Mn_{1/2}$]O_2 and Li[$Ni_{1/3}Li_{1/9}Mn_{5/9}$]O_2 samples. The experimental [$\bar{1}$11]$_{hex.}$ and [00$\bar{1}$]$_{hex.}$ patterns collected from the Li_2MnO_3 sample were compared to the simulated electron diffraction patterns of the $\sqrt{3}\boldsymbol{a}_{hex.} \times \sqrt{3}\boldsymbol{a}_{hex.} \times \boldsymbol{c}_{hex.}$ superstructure and the conventional monoclinic structure along the equivalent zone axes, as shown in Figure 10a−f, respectively. The superlattice reflections (marked by open circles) present in the experimental patterns in Figure 10a and d can be indexed to the $\sqrt{3}\boldsymbol{a}_{hex.} \times \sqrt{3}\boldsymbol{a}_{hex.} \times \boldsymbol{c}_{hex.}$ superstructure with space group $P3_112$, as evidenced in the simulated electron diffraction patterns (using the Cerius[2] program) along the equivalent zone axes in Figure 10b and e, respectively. However, either none or only some of the superlattice reflections (marked by open circles) observed in the experimental patterns were found in the simulated patterns of the monoclinic structure with space group $C2/m$, as shown in Figure 10c and f. It is believed that the extra reflections (marked by short lines) present in Figure 10d result from the double diffraction effect in the transmission electron microscope.

Proposed Cation Arrangements in Li[$Ni_xLi_{1/3-2x/3}$-$Mn_{2/3-x/3}$]O_2 ($0 \le x \le 1/2$). *In-Plane Ordering.* It was found that in-plane $\sqrt{3}\boldsymbol{a}_{hex.} \times \sqrt{3}\boldsymbol{a}_{hex.}$ ordering (shown in Figure 2) existed in all three samples of the Li[$Ni_xLi_{1/3-2x/3}Mn_{2/3-x/3}$]$O_2$ series and the intensities of superlattice reflections decreased as the lithium content in the transition metal layer was reduced. Given the $Li_{1/3}Mn_{2/3}$ composition of the transition

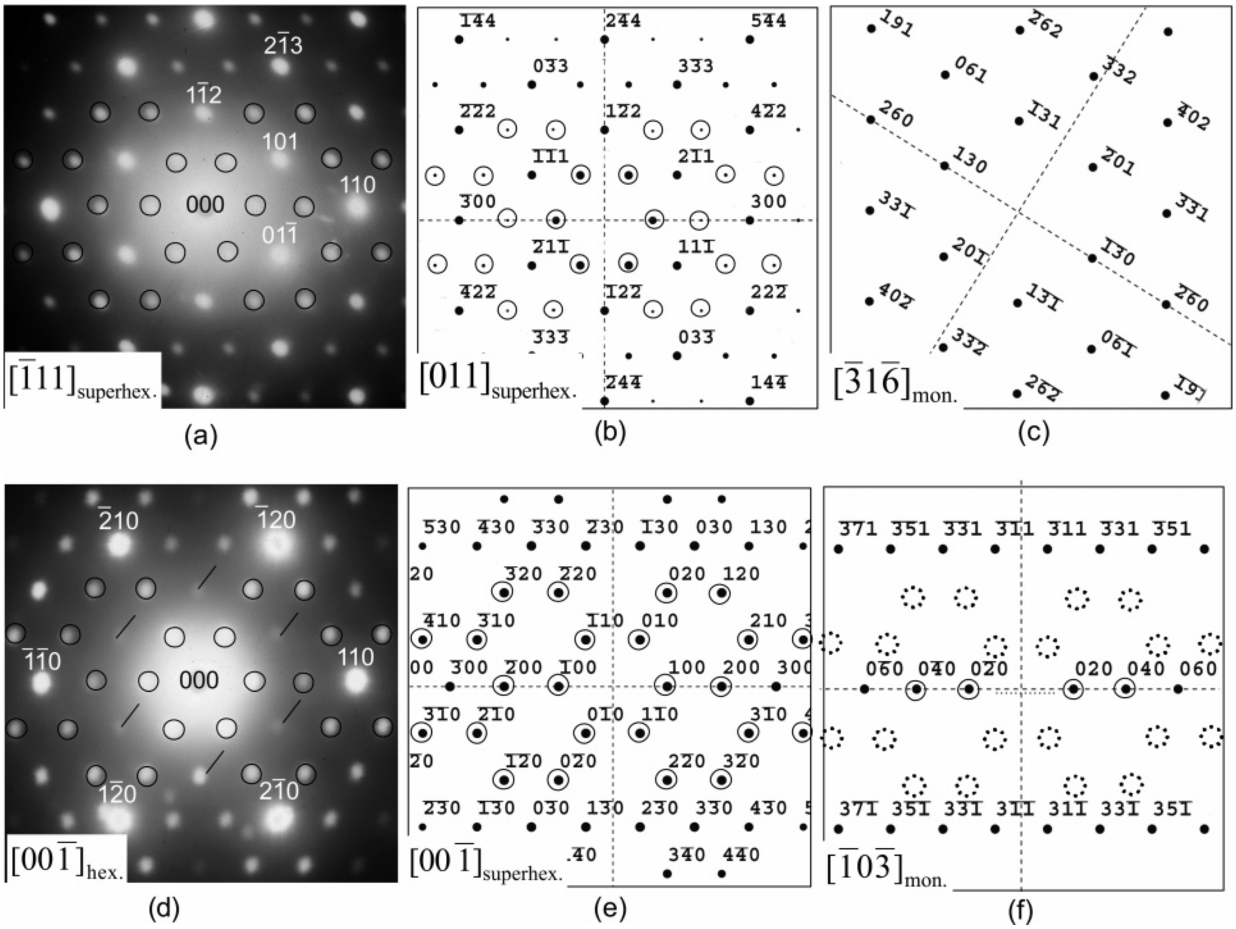

Figure 10. (a) Experimental $[\bar{1}11]_{hex.}$ electron diffraction pattern collected from the Li_2MnO_3 sample, (b) the simulated $[011]_{superhex.}$ pattern of the superstructure with space group $P3_112$, (c) the simulated $[\bar{3}1\bar{6}]_{mon.}$ pattern of the monoclinic structure of Li_2MnO_3 with space group $C2/m$, (d) the experimental $[00\bar{1}]_{hex.}$ electron diffraction pattern collected from the Li_2MnO_3 sample, (e) the simulated $[00\bar{1}]_{superhex.}$ pattern of the superstructure with space group $P3_112$, and (f) the simulated $[\bar{1}0\bar{3}]_{mon.}$ pattern of the monoclinic structure of Li_2MnO_3 with space group $C2/m$.

Table 3. Average Occupancies of α and β Sites and the Long-Range Ordering Parameter in $Li[Ni_xLi_{1/3-2x/3}Mn_{2/3-x/3}]O_2$ Compounds ($0 \leq x \leq {}^1/_2$) Vary with the Lithium Fraction in the Transition Metal Layers

nominal composition	$Li[Ni_{1/2}Mn_{1/2}]O_2$	$Li[Ni_{1/3}Li_{1/9}Mn_{5/9}]O_2$	Li_2MnO_3
transition metal layer	$Li_{0.11}Ni_{0.39}Mn_{0.50}$	$Li_{0.17}Ni_{0.28}Mn_{0.55}$	$Li_{0.33}Mn_{0.67}$
z_{Li}	$\sim{}^1/_9$	$\sim{}^1/_6$	${}^1/_3$
proposed average occupancies $\alpha:\beta = 1:2$	α (0.33 Li; 0.67 Ni) β (0.75 Mn; 0.25 Ni)	α (0.51 Li; 0.49 Ni) β (0.82 Mn; 0.18 Ni)	α (1.00 Li) β (1.00 Mn)
long range ordering parameter S [a]	33%	51%	100%

[a] $S = (\gamma_a - z_{Li})/Y_\beta$ where γ_α is the fraction of α sites occupied by Li^+, and Y_β is the fraction of β sites on the trigonal lattice.

metal layer in Li_2MnO_3, the occupation of α and β sites are stiochiometric (all Li^+ on α and all Mn^{4+} on β), where the long-range order parameter S reaches unity.[27] As Ni^{2+} substitutes for Li^+ or Li^+ and Mn^{4+} on the trigonal lattice, one cannot create a stoichiometric occupation of α and β sites in the transition metal layer. However, this does not preclude long-range ordering, which is quite common with partial occupancies having long-range order parameter S less than unity.[27] As Li^+ and Mn^{4+} order onto respective α and β sublattices, and first-principles studies suggest the ordering tendency of Ni^{2+} and Mn^{4+}, it is believed that the maximum ordering between Ni^{2+} and Mn^{4+} occurs when Ni^{2+} ions preferentially occupy α sites. A likely model for the occupancies on the α and β sublattices in the transition metal layer of the $Li[Ni_{1/2}Mn_{1/2}]O_2$, $Li[Ni_{1/3}Li_{1/9}Mn_{5/9}]O_2$, and Li_2MnO_3 samples is proposed, as listed in Table 3. It should be noted that the long-range order parameter S decreases from unity in Li_2MnO_3 to 33% in $Li[Ni_{1/2}Mn_{1/2}]O_2$ as the lithium fraction in the transition metal layer decreases. As the intensities of the superstructure reflections are proportional to S^2, the superstructure peak intensities should decrease sharply with reducing lithium fraction in the transition metal layer, which is consistent with experimental synchrotron X-ray diffraction and electron diffraction observations (Figures 6 and 7).

Given strong electrostatic interactions between Li^+ and Mn^{4+} and the stoichiometric ratio of $Li^+/Mn^{4+} = 1:2$ in the transition metal layer, in-plane $\sqrt{3}a_{hex.} \times \sqrt{3}a_{hex.}$ ordering in Li_2MnO_3 is expected to be nearly perfect. It is believed that the formation of antiphase boundaries in the transition metal layer of Li_2MnO_3 is energetically unfavorable. As the lithium fraction in the transition metal layer decreases, it is

---

(27) Warren, B. E. *X-ray Diffraction*; Dover Publications: New York, 1990.

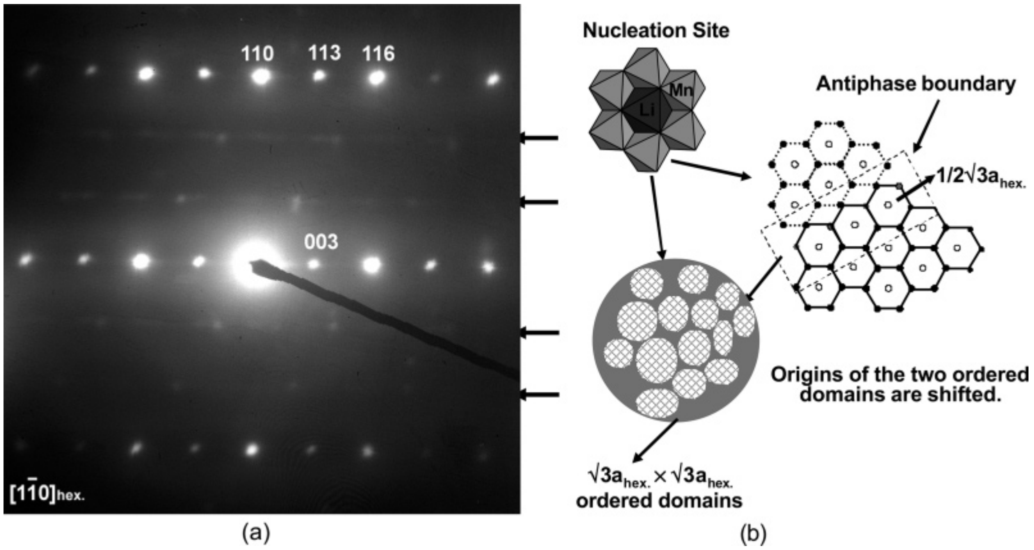

Figure 11. (a) Electron diffraction pattern along the $[1\bar{1}0]_{\text{hex.}}$ zone axis collected from the $Li[Ni_{1/2}Mn_{1/2}]O_2$ sample. The streaking perpendicular to the (110) plane normal reveals that the sizes of ordered domains in the transition metal layers are small. (b) A microstructure that consists of multiple $\sqrt{3}\boldsymbol{a}_{\text{hex.}} \times \sqrt{3}\boldsymbol{a}_{\text{hex.}}$ ordered domains grown from different $LiMn_6$ nuclei and antiphase boundaries is proposed.

suggested that the coherent length for in-plane $\sqrt{3}a_{\text{hex.}} \times \sqrt{3}a_{\text{hex.}}$ ordering will be reduced. In the $Li[Ni_{1/3}Li_{1/9}Mn_{5/9}]O_2$ sample that had 51% of α sites occupied by Li^+, the in-plane ordering was still very pronounced as evidenced by the presence of superstructure peaks in the X-ray spectrum (Figure 7) and superstructure reflections in all of the electron diffraction patterns collected. In contrast, in the $Li[Ni_{1/2}Mn_{1/2}]O$ sample with 33% of α sites occupied by Li^+, long-range $\sqrt{3}\boldsymbol{a}_{\text{hex.}} \times \sqrt{3}\boldsymbol{a}_{\text{hex.}}$ ordering (superstructure reflections) was found only in 50% of the crystals analyzed by electron diffraction. Moreover, ordered domains on the order of a few nanometers (coherence length for in-plane ordering) were found, as evidenced by the streaking perpendicular to the $(110)_{\text{hex.}}$ normal in Figure 11a. It is believed that multiple ordered domains grown from different $LiMn_6$ nuclei can coexist in individual crystals of the $Li[Ni_{1/2}Mn_{1/2}]O_2$ sample, as shown in Figure 11b. Such a domain microstructure was recently reported and revealed by high-resolution transmission electron microscopy and local fast Fourier analysis.[13] The boundaries of these ordered domains can be described as antiphase boundaries and one example having the lattice origins shifted by ${}^1/_2\sqrt{3}\boldsymbol{a}_{\text{hex.}}$ along the $\boldsymbol{a}_{\text{hex.}}$ direction) is shown in Figure 11b.

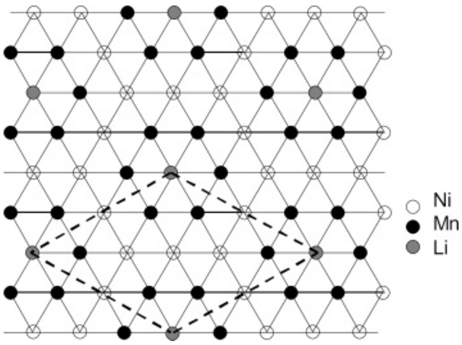

Figure 12. $2\sqrt{3}\boldsymbol{a}_{\text{hex.}} \times 2\sqrt{3}\boldsymbol{a}_{\text{hex.}}$ superstructure and the stoichiometric composition of the transition metal layer in this flower ordering arrangement is $Li_{1/12}Ni_{5/12}Mn_{1/2}$.[28]

With low lithium fraction in the transition metal layer, lithium ions can order in sublattices greater than the $\sqrt{3}\boldsymbol{a}_{\text{hex.}} \times \sqrt{3}\boldsymbol{a}_{\text{hex.}}$ supercell. Recently a $2\sqrt{3}\boldsymbol{a}_{\text{hex.}} \times 2\sqrt{3}\boldsymbol{a}_{\text{hex.}}$ superstructure model for the $Li[Ni_{1/2}Mn_{1/2}]O_2$ composition having a stoichiometric occupancy of $Li_{1/12}Ni_{5/12}Mn_{1/2}$ in the transition metal layer has been proposed from first-principles studies,[28] as shown in Figure 12. In this superstructure, the center of the small honeycomb on the triangular lattice is occupied by Li^+ (light gray circles) surrounded by 6 Mn^{4+} (black circles) as the nearest neighbors and each small honeycomb is surrounded by 12 Ni^{2+} (open circles), which forms a "flower" ordering arrangement. As the $Li[Ni_{1/2}Mn_{1/2}]O_2$ sample (heat-treated at 900 °C) used in this study had a lithium content of 11% in the transition metal layer, considerably higher than the stoichiometric lithium fraction (8.3%) required for this superstructure, the formation of the $2\sqrt{3}\boldsymbol{a}_{\text{hex.}} \times 2\sqrt{3}\boldsymbol{a}_{\text{hex.}}$ superstructure was precluded. As it was reported that $Li[Ni_{1/2}Mn_{1/2}]O_2$ samples heat-treated at 1000 °C had lower lithium fractions (7.8%) in the transition metal layer than those obtained at 900 °C,[3] electron diffraction studies should be performed on $Li[Ni_{1/2}Mn_{1/2}]O_2$samples heat-treated at 1000 °C to verify the existence of the "flower" ordering arrangement.

Stacking Sequence of Ordered Planes. In principle, there may exist an infinite number of possible ways how the in-plane $\sqrt{3}\boldsymbol{a}_{\text{hex.}} \times \sqrt{3}\boldsymbol{a}_{\text{hex.}}$ ordered planes can be stacked perpendicular to the layers (along the $\boldsymbol{c}_{\text{hex.}}$ axis). It is important to point out that the same in-plane ordering but different stacking of the ordered planes could lead to different crystal symmetry and space groups as reported by Lang.[29] The difference in the layered structures with space group $P3_112$ and $C2/m$ is demonstrated by stacking three successive, ordered transition metal layers projected along the $\boldsymbol{c}_{\text{hex.}}$ direction, as shown in Figure 13, where only α sites are shown for each transition metal layer. The $P3_112$ structure has a 3-fold screw axis while the $C2/m$ structure has a 2-fold

---

(28) Van der Ven, A.; Ceder, G. *Electrochem. Commun.* **2004**, *6*, 1045−1050.

(29) Lang, G. *Z. Anorg. Allg. Chem.* **1966**, *348*, 246−249.

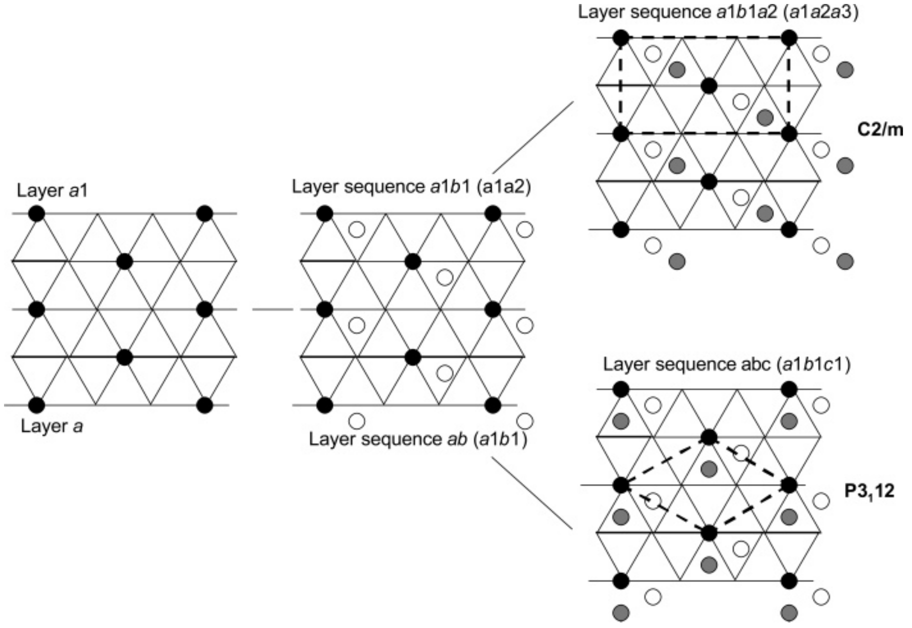

Figure 13. Stacking sequences of in-plane $\sqrt{3}\boldsymbol{a}_{\mathrm{hex.}} \times \sqrt{3}\boldsymbol{a}_{\mathrm{hex.}}$ ordered planes to structures with space group $C2/m$ and $P3_112$. Note that only *a* sites are shown and the supercells are outlined by dashed lines.

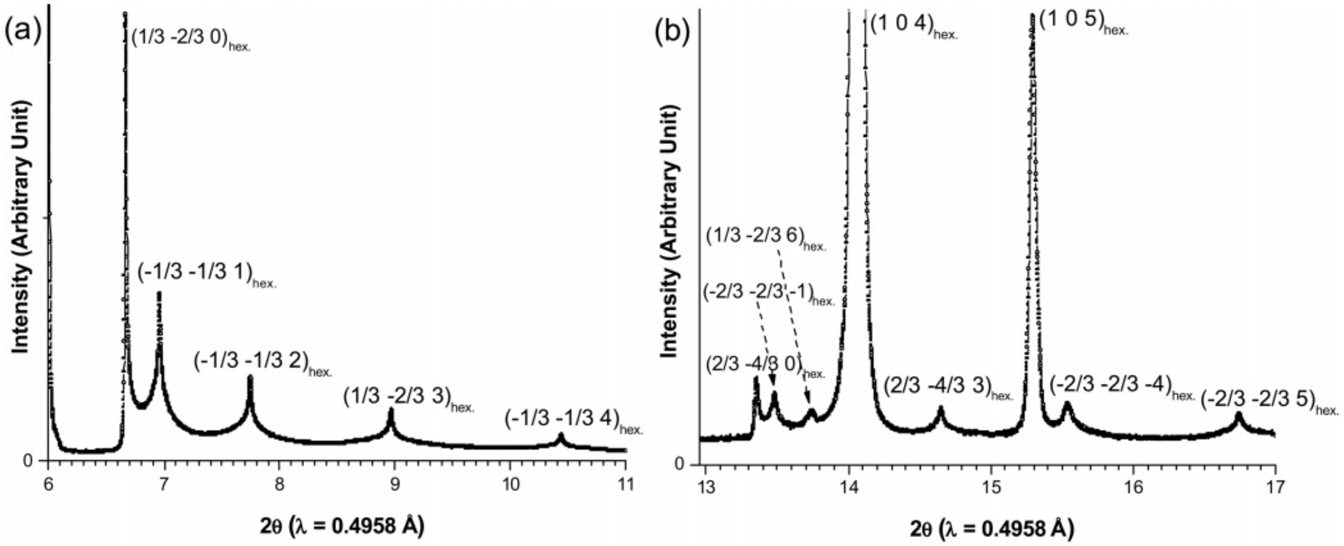

(c) Proposed disorder in the stacking sequence of $Li_{1/3}Mn_{2/3}$ layers in Li_2MnO_3

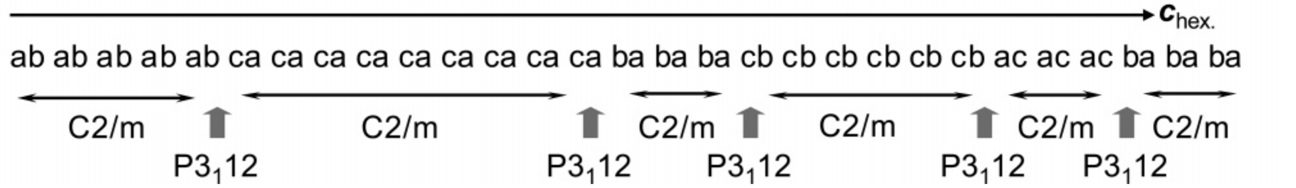

Figure 14. (a) and (b) Regions of synchrotron X-ray powder diffraction data of the Li_2MnO_3 sample show the broadening of selective superstructure peaks, which are reindexed to the parent hexagonal structure having space group $R\bar{3}m$. Note that the $(hk0)_{\mathrm{hex.}}$ reflections are much sharper than the $(hkl)_{\mathrm{hex.}}$ ones. (c) An example of the disorder in the stacking sequence of $Li_{1/3}Mn_{2/3}$ layers in the layered Li_2MnO_3 structure is shown.

axis parallel to the $\boldsymbol{c}_{\mathrm{hex}}$ axis. Although electron diffraction data of the $Li[Ni_xLi_{1/3-2x/3}Mn_{2/3-x/3}]O_2$ ($x = {}^1/_2$, ${}^1/_3$, and 0) crystals could be indexed to the $\sqrt{3}\boldsymbol{a}_{\mathrm{hex.}} \times \sqrt{3}\boldsymbol{a}_{\mathrm{hex.}} \times \boldsymbol{c}_{\mathrm{hex.}}$ superstructure with space group $P3_112$, it is important to point out that electron diffraction results cannot preclude the presence of some transition metal layers with the $C2/m$ stacking sequence in the individual crystals analyzed. Therefore, it is believed that the transition metal layers in the layered $Li[Ni_xLi_{1/3-2x/3}Mn_{2/3-x/3}]O_2$ compounds can be arranged in the following ways: (1) mostly in the $P3_112$ stacking with some $C2/m$ stacking abnormally, and (2) in two or three different $C2/m$ stacking sequence variants (*abab*..., *caca*..., and *cbcb*...) along the $\boldsymbol{c}_{\mathrm{hex.}}$ axis. The presence of nickel in the lithium layer between two adjacent transition metal layers could play an important role in how the transition metal layers of $Li[Ni_{1/2}Mn_{1/2}]O_2$ and $Li[Ni_{1/3}Li_{1/9}Mn_{5/9}]O_2$

crystals are stacked along the $\boldsymbol{c}_{\text{hex.}}$ axis. It is believed that the $P3_112$ stacking might be preferred to the $C2/m$ type as the nickel fraction in the lithium layer increases to minimize the electrostatic repulsion between the lithium ions in the transition metal layer and the nickel ions in the lithium layers above and/or below. As there is no nickel in the lithium layer of the Li_2MnO_3 sample and previous single-crystal X-ray diffraction studies have revealed that Li_2MnO_3 should have the $C2/m$ stacking sequence,[20] it is speculated that stacking abnormally (any deviation from the ideal $C2/m$ stacking sequence) of ordered $Li_{1/3}Mn_{2/3}$ layers is present in the Li_2MnO_3 sample analyzed in this study, where two or three different $C2/m$ stacking sequence variants coexist along the $\boldsymbol{c}_{\text{hex.}}$ axis. Such disorder in the stacking (packing if the layers are closed-packed) of successive layers has been reported in several previous studies.[30−32] We further discuss the disorder in the stacking sequence of ordered layers in the Li_2MnO_3 sample in the following section.

Disorder in the Stacking Sequence of Ordered Planes in Li_2MnO_3. Profile matching of the synchrotron data of the Li_2MnO_3 sample prepared at 850 °C has shown that the monoclinic structure is not fully relaxed having the $a_{\text{mon.}}/b_{\text{mon.}}$ ratio and β angle closer to the ideal value than those reported previously.[20,21] It is believed that the level of monoclinic distortion might be correlated with the extent of stacking disorder along the $\boldsymbol{c}_{\text{hex.}}$ axis as the layered structure accommodates strain associated with shearing of oxygen lattice (the deviation from the ideal β value) and electrostatic interactions of in-plane Li^+ and Mn^{4+} ordering (the deviation from the ideal $a_{\text{mon.}}/b_{\text{mon.}}$ ratio). In addition, the $(hkl,\ l \neq 0)_{\text{hex.}}$ superstructure peaks are broadened significantly while the $(hk0)_{\text{hex.}}$ superstructure reflections remain sharp, as shown in Figure 14, in which the superstructure reflections of the monoclinic Li_2MnO_3 structure are reindexed to the parent hexagonal structure. It is believed that selective broadening of the $(hkl,\ l \neq 0)_{\text{hex.}}$ superstructure peaks is attributed to disorder in the stacking sequence of ordered $Li_{1/3}Mn_{2/3}$ arrangements along the $\boldsymbol{c}_{\text{hex.}}$ axis. One example of proposed disorder in the stacking sequence of ordered $Li_{1/3}Mn_{2/3}$ layers in Li_2MnO_3 is shown in Figure 14c, where several different $C2/m$ stacking sequence variants coexist along the $\boldsymbol{c}_{\text{hex.}}$ axis. One or multiple cells of $P3_112$ form along the $\boldsymbol{c}_{\text{hex.}}$ axis, where stacking abnormally in the $C2/m$ sequence occurs. Such arrangement of transition metal layers is consistent with the experimental electron diffraction patterns collected from the Li_2MnO_3 sample. The effect of the disorder in the stacking sequence on the X-ray powder and single-crystal electron diffraction patterns of Li_2MnO_3 samples is being investigated using DIFFaX[33] and will be reported in a future paper.

Acknowledgment. We thank Peter Lee from Argonne National Laboratory and Sundeep Kumar from MIT for their assistance in synchrotron X-ray diffraction data collection and refinements. This work was supported in part by the Assistant Secretary for Energy Efficiency and Renewable Energy, Office of FreedomCAR and Vehicle Technologies of the U.S. Department of Energy via subcontracts 6517749 and 6517748, the MRSEC Program of the National Science Foundation under award DMR 02-13282, and the Singapore-MIT Alliance. Y. S.-H. acknowledges the Office of Naval Research Young Investigator Award N00014-03-10448 for financial support and fruitful discussions with Laurence Croguennec at ICMCB-CNRS in Bordeaux, France.

CM047779M

---

(30) Muller, F.; Plancon, A.; Besson, G.; Drits, V. A. *Mater. Struct.* **1999**, *6*, 129−134.

(31) Thiel, J. P.; Chiang, C. K.; Poeppelmeier, K. R. *Chem. Mater.* **1993**, *5*, 297−304.

(32) Jorgensen, J. D.; Avdeev, M.; Hinks, D. G.; Burley, J. C.; Short, S. *Phys. Rev. B* **2003**, *68*, 214517.

(33) Treacy, M. M. J.; Newsam, J. M.; Deem, M. W. *Proc. R. Soc. London Ser. A* **1991**, *43*, 499−520.